analytical chemistry

pubs.acs.org/ac Article

A Strategy for the Determination of Alkaline Phosphatase Based on the Self-Triggered Degradation of Metal−Organic Frameworks by Phosphate

Wei Wang, Jingkang Li, Yibing Liu, Wei Zhang, Ying Sun, Pinyi Ma,* and Daqian Song*

Cite This: *Anal. Chem.* 2023, 95, 3414−3422 Read Online

ACCESS | Metrics & More | Article Recommendations | Supporting Information

ABSTRACT: Alkaline phosphatase (ALP) is widely present in the human body and is an important biomarker. Numerous ALP detection studies have been carried out, and ascorbic acid (AA) is often used as the reducing component in the sensors to monitor ALP levels since it can be produced from ascorbic acid 2-phosphate (AA2P) hydrolysis in the presence of ALP. However, it is well-known that AA is a strong reducing agent and can be easily oxidized. The disproportion between oxidized AA and reduced AA reactions results in the generation of AA free radicals with single electrons that may lead to inaccurate results in assays. To solve this problem, we synthesized a core−shell metal−organic framework sensor (PATP-Au@ZIF-8 NP) and used it as a sensitive and accurate ALP detection sensor with self-triggered control of phosphate ions (Pi) to avoid the potential inaccuracy of the method that uses AA as the reducing component. By establishing a physical shell on the surface of the gold nanoparticles (Au NPs), the sensor not only can eliminate the random assembly of metal nanoparticles caused by plasma exposure but also can generate self-triggering of Pi caused by ALP. Pi can decompose ZIF-8 through coordination with Zn^{2+} and thus can destroy the ZIF-8 shell structure of the prepared PAZ NPs. Au NPs are released and then become aggregated, in turn causing the SERS "hot spot" area to increase. The enhancement of the SERS signals was found to be directly associated with the level of Pi released from ALP-triggered hydrolysis. The response of the strategy was linear at ALP concentrations ranging from 0.1 to 150 mU/mL (r = 0.996) with a detection limit of 0.03 mU/mL. Lastly, the developed strategy was employed in the evaluation of ALP inhibitors, and the possibility to implement the developed SERS strategy for rapid and selective analysis of ALP in human serum was demonstrated.

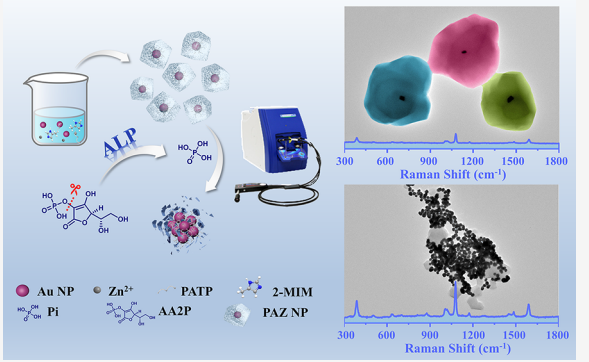

INTRODUCTION

Alkaline phosphatase (ALP), an enzyme first discovered in the 1920s, has been considered as a potential biomarker of many disorders.[1−4] Measuring its activity level in human serum is usually carried out during the diagnosis of bone disease,[5] diabetes,[6] liver dysfunction,[7] leukemia,[8] and other related diseases. Therefore, the sensitive, rapid, and simple determination of ALP is of great significance for the clinical diagnosis of ALP-related diseases.

To date, many methods including colorimetry,[9] electrochemistry,[10] electrochemiluminescence (ECL),[11] fluorometry,[12] and surface-enhanced Raman methods[13,14] have been used to construct ALP biosensors. Among all methods, surface-enhanced Raman scattering (SERS) is a widely used method due to its advantages of short analysis time, high sensitivity, and simple operation.[15,16] The complex composition, variable configuration, and small scattering cross section of the enzyme bring great difficulty to directly acquire and accurately analyze its SERS spectrum. To solve this problem, researchers have constructed SERS sensors that can specifically react with the target analyte to detect the enzyme based on the changes in the SERS spectrum before and after the reaction.[17,18] Numerous strategies have used ascorbic acid (AA) as a reducing component in sensor design to extend the capability of the sensor to monitor some other disease biomarkers, such as ALP.[19,20] For example, Xi et al. designed a SERS sensor based on the response of Au NP surface-modified 2-mercaptoquinone (2-MBQ) to AA formed by dephosphorylation of ascorbic acid 2-phosphate (AA2P) in the presence of ALP.[21] Similarly, AA produced by hydrolysis of AA2P in the presence of ALP can reduce MnO_2 to Mn^{2+}, which can etch the outer shell of gold nanobipyramids@MnO_2 nanoparticles (AMNS). Liu et al. quantified the ALP activity based on the Raman

Received: November 15, 2022
Accepted: January 20, 2023
Published: January 30, 2023

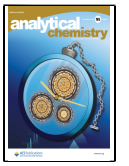

https://doi.org/10.1021/acs.analchem.2c05098
Anal. Chem. 2023, 95, 3414−3422

Scheme 1. The Principle of the Determination of ALP Based on the Self-Triggered Degradation of Metal−Organic Frameworks by Phosphate

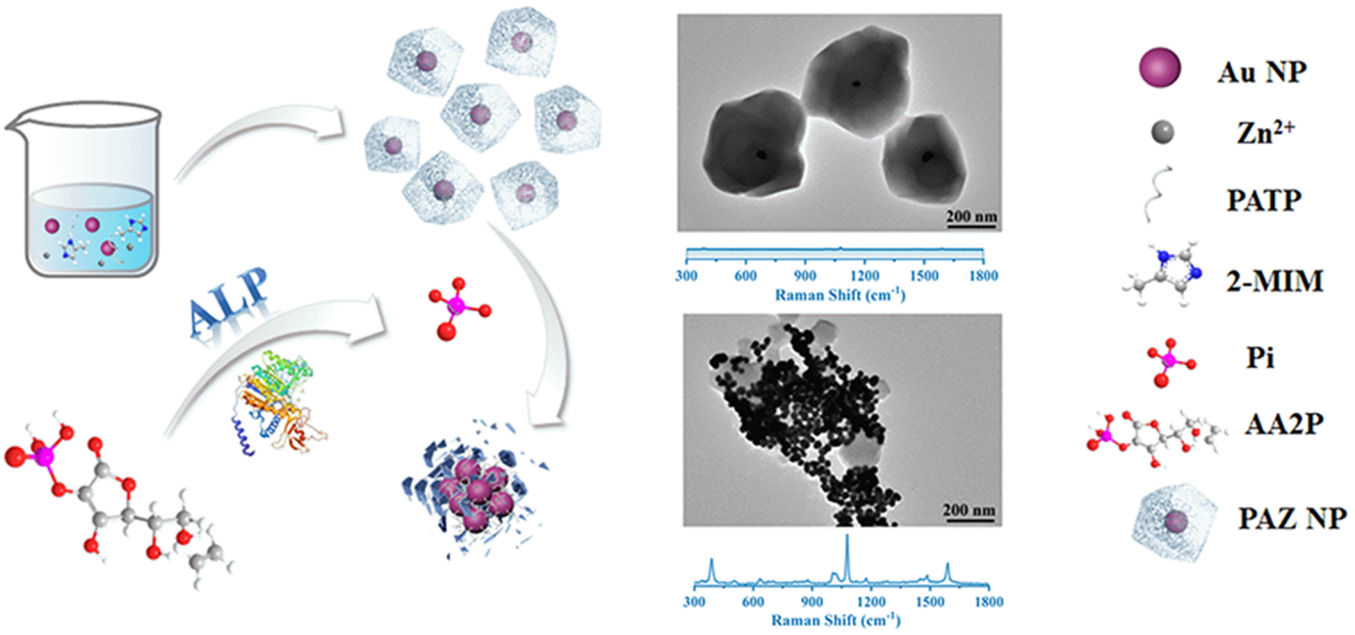

signal, which varies with the thickness of the MnO_2 shell.[22] It is well-known that AA is a strong reducing agent that can scavenge free radicals. However, in an in vitro system, AA is easily oxidized, and when the disproportion between the content of oxidized and reduced AA occurs, it results in the generation of AA free radicals with single electrons.[23−25] This process then leads to inaccuracy of the in vitro detection results, which is not conducive to the detection of biomarkers of certain diseases by methods that use AA as the reducing component.

Nevertheless, SERS assays are not able to circumvent some disadvantages of the SERS system such as the stability when analyzing complex samples. The exposed plasmonic metal matrices are susceptible to random aggregation due to certain factors, such as pH, ionic strength, etc.,[26,27] which can seriously affect the accuracy of the SERS assay. To solve this problem, an effective solution is to build a physical shell (such as ZIF-8) on the noble metal surface to restrict their direct collisions. Zeolite imidazole framework (ZIF-8) materials are members of metal−organic frameworks (MOFs) that have good biocompatibility and chemical stability and can be simply and rapidly synthesized and easily functionalized. They are widely used in catalysis,[28] sensors,[29] drug transportation, and other fields.[30,31] The problem in random aggregation can be effectively solved by wrapping ZIF-8, as a shell, on the outer layer of plasmonic metal matrices to construct SERS substrates. It has been reported that the degradation of ZIF-8 occurs under certain conditions, such as in a phosphate solution.[32,33] The degradation rate in a phosphate solution is faster and at a higher degree than that in a water environment due to the presence of moieties that have high affinity to the released building block of ZIF-8 (i.e., Zn^{2+} and MIM^-) such as phosphate ions.

Therefore, we proposed a sensitive and accurate ALP detection method based on self-triggered control to avoid the potential inaccuracy of the detection method that uses AA as the reducing component (Scheme 1). We synthesized a core−shell metal−organic framework sensor (PATP-Au@ZIF-8 NPs (PAZ NPs)). By establishing a physical shell on the surface of the gold nanoparticles (Au NPs), the sensor not only can eliminate the random assembly of metal nanoparticles caused by plasma exposure but also can induce self-triggering of Pi by ALP. Pi can decompose ZIF-8 through coordination with Zn^{2+} and thus can destroy the ZIF-8 shell structure of the prepared PAZ NPs. Au NPs are released and then become aggregated, leading to the increase of the SERS "hot spot" area. The enhancement of the SERS signal positively correlates with the Pi content released by self-triggered hydrolysis of ALP. Finally, the developed strategy was employed to evaluate ALP inhibitors.

EXPERIMENTAL PROCEDURES

Synthesis of Au NPs and PATP-Au NPs. According to the previous Frens' method, Au NPs with a particle size of about 28 nm were synthesized. The ZIF-8 coating of individual metal nanoparticles was based on a previously reported protocol with slight modifications. The detailed synthesis procedures are available in the Supporting Information (Figure S1).

Phosphate-Controlled Collapse of ZIF-8. The as-prepared PAZ NPs and PBS solution were incubated with HEPES buffer solution for 20 min at room temperature. The difference in SERS intensity with the different concentrations of PBS at 1075 cm^{-1} was observed to monitor the release of PATP-Au NPs. The detailed procedures are available in the Supporting Information.

Selectivity Evaluation and Anti-interference Experiments. Some potential interfering molecules, including ions, enzymes, and biomolecules, were used in the selectivity evaluation and anti-interference experiments of the assay; details are given in the Supporting Information.

Determination of ALP in Serum. Serum samples, AA2P, and PAZ NP solution were added into HEPES buffer solution containing $MgCl_2$. After incubating at 37 °C for 50 min, the mixture solution was prepared for SERS measurements. The

https://doi.org/10.1021/acs.analchem.2c05098
Anal. Chem. 2023, 95, 3414−3422

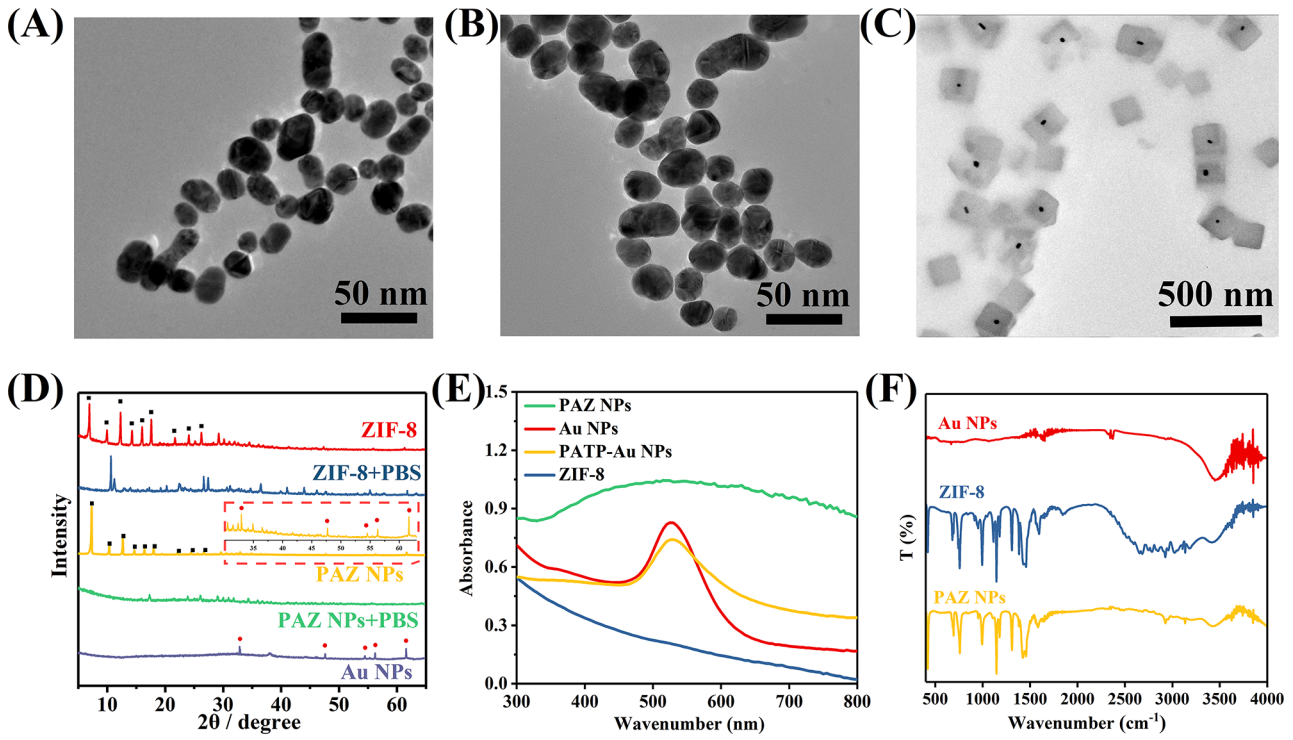

Figure 1. TEM images of Au NPs (A), PATP-Au NPs (B), and PAZ NPs (C). XRD patterns of ZIF-8, ZIF-8+PBS, PAZ NPs, PAZ NPs+PBS, and Au NPs (D). UV−visible absorption spectra of PAZ NPs, Au NPs, PATP-Au NPs, and ZIF-8 (E). FTIR spectra of Au NPs, ZIF-8, and PAZ NPs (F).

detailed SERS determination procedures are available in the Supporting Information.

Evaluation of the ALP Inhibitor. To confirm its effectiveness in screening inhibitors, the proposed strategy was employed to screen the ALP inhibitor (Na_3VO_4). The Na_3VO_4 aqueous solution and the ALP aqueous solution of different concentrations were mixed and reacted in a water bath at 37 °C for 30 min. The next steps were the same as in the section "Determination of ALP in Serum". The detailed procedures are available in the Supporting Information.

RESULTS AND DISCUSSION

Synthesis and Characterization of PAZ NPs. The synthesis procedures are shown in Figure S1. Cetyltrimethyl ammonium bromide (CTAB) was added during various steps of the synthesis process: the addition of CTAB during the synthesis of Au NPs can increase the dispersibility of Au NPs so that they can be better wrapped with the ZIF-8 shell during the next step.[34] Without CTAB, Au NPs tend to aggregate and cannot form an ideal structure when wrapping ZIF-8 (Figure S2). During the synthesis of ZIF-8, the addition of CTAB can adjust the size of ZIF-8. The addition of CTAB during the synthesis of PAZ NPs not only can increase the dispersibility of PATP-Au NPs but also can adjust the size of PAZ NPs. Here, we utilized the ionic surfactant CTAB to bridge between the metal and ZIF-8 surfaces and to facilitate the controlled alignment. This molecular layer of CTAB acts as a hydrophobic tail to bridge the interaction between metals and ZIF-8, as well as to stabilize specific facets of the metals and MOFs; thus, the alignment between the crystal structures of the cores and the shells can be expected.

As illustrated in Figure 1A, the average size of Au NPs was 28 nm, and the aqueous suspension of Au NPs had a red wine color (Figure S6) with an absorbance at 529 nm (Figure 1E). The TEM image of PATP-Au NPs is shown in Figure 1B. As can be seen in Figure 1C, PAZ NPs were successfully encapsulated in Au NPs and ZIF-8. In addition, the absorbance of PATP-Au NPs was not significantly changed, indicating that the surface plasmon resonance effect of Au NPs was unchanged after modification. ZIF-8 did not exhibit a surface plasmon absorption peak, and its solution was white and turbid (Figure S6). The suspension of PAZ NPs was purple and turbid (Figure S6), which is consistent with that reported in the literature,[34] and exhibited a broad plasma absorption peak at 510 nm. Compared with that of Au NPs, the PAZ NPs exhibited broad surface plasmonic resonance (SPR) peaks that are in agreement with those reported in the literature.[35] Additionally, the surface plasmon peak position of PAZ NPs was slightly redshifted. The redshift is believed to be caused by the change in the dielectric constant of ZIF-8 coated on Au NPs, which caused the position of the absorption peak of nanoparticles to change.

X-ray diffraction (XRD) was employed to evaluate the crystallinity of ZIF-8, Au NPs, and PAZ NPs (Figure 1D). The synthesized ZIF-8 exhibited a typical ZIF-8 diffraction pattern, which is the indication that ZIF-8 was successfully synthesized. The XRD patterns of PAZ NPs were in agreement with those of ZIF-8 and Au NPs. This implies that Au NPs were successfully encapsulated in ZIF-8 without breaking its crystalline structure. It can be seen from Figure 1D that the (011) plane of ZIF-8 and PAZ NP crystals disappeared upon the addition of PBS, indicating that PBS can destroy the crystal structure of ZIF-8.

Then, we measured the Fourier transform infrared (FTIR) absorption spectra of the nanoparticles, as shown in Figure 1F. The presence of these vibration bands ($\nu_{C=N}$, 1582 cm^{-1}; ν_{ring},

https://doi.org/10.1021/acs.analchem.2c05098
Anal. Chem. 2023, 95, 3414−3422

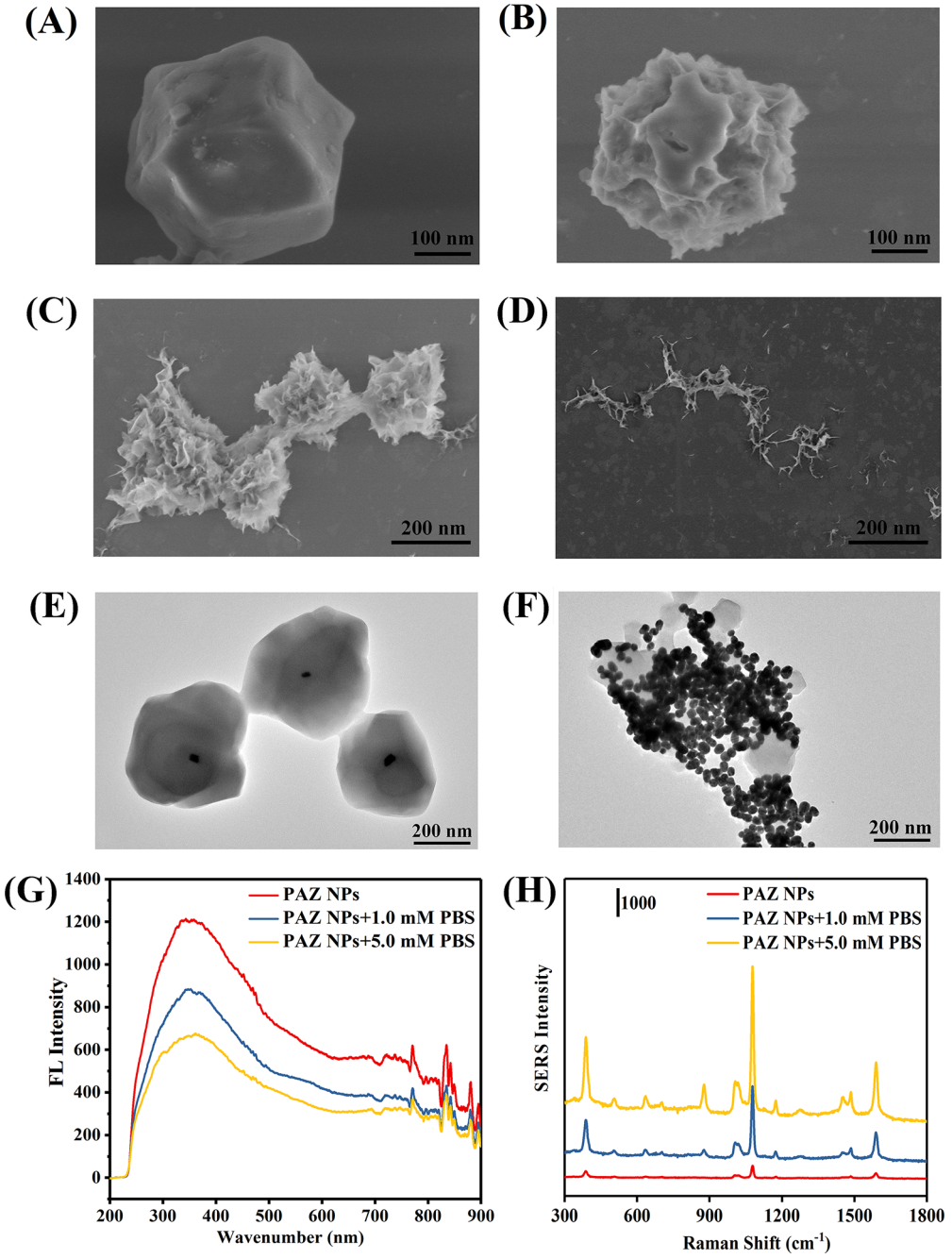

Figure 2. SEM images showing morphological changes of ZIF-8 particles after the addition of different concentrations of PBS (0, 0.5, 1, and 5 mM) (A–D). TEM images of PAZ NPs (E) and PAZ NPs+PBS (2 mM) (F). Synchronous fluorescence spectra of PAZ NPs in PBS at different concentrations (the excitation and emission wavelengths in the range from 200 to 900 nm) (G). SERS spectra of PAZ NPs in PBS at different concentrations (H).

1500–1350 cm^{-1}; $\delta_{\text{out-of-plane bending}}$, 800–650 cm^{-1}; and $\nu_{\text{Zn–N stretching}}$, 421 cm^{-1}) confirms the successful formation of the ZIF-8 framework.[34] In addition, the FTIR spectrum of PAZ NPs is consistent with that of ZIF-8, indicating that Au NPs were successfully encapsulated in ZIF-8 without breaking its crystalline structure.

Figure S3 shows the SERS spectra of PATP-Au NPs and PAZ NPs. The spectra showed main peaks at 390, 505, 635, 701, 1005, 1079, 1174, 1487, and 1591 cm^{-1}, which are characteristic peaks of chemisorbed PATP molecules. The spectrum of PATP-Au NPs was different from that of PAZ NPs at 876, 1014, and 1451 cm^{-1}. Based on previous reports,[36,37] the peak observed at 876 and 1014 cm^{-1} corresponds to the stretching of ring C–H in methyl groups, while that at 1451 cm^{-1} corresponds to the stretching of ring C–N and the bending of N–H in 2-methylimidazole (2-MIM). The difference between the spectra suggests that there are interactions between 2-MIM and Au NPs. The quantitative analysis of ALP was established based on the peak area of the characteristic peak of PATP at 1075 cm^{-1}.

Control of ZIF-8 Collapse and PATP-Au NP Release by Pi. We further demonstrated that Pi could destroy ZIF-8. We found that in HEPES buffer (5 mM, pH = 8.5), ZIF-8 could not be etched, and the buffer had no effect on the

https://doi.org/10.1021/acs.analchem.2c05098
Anal. Chem. 2023, 95, 3414–3422

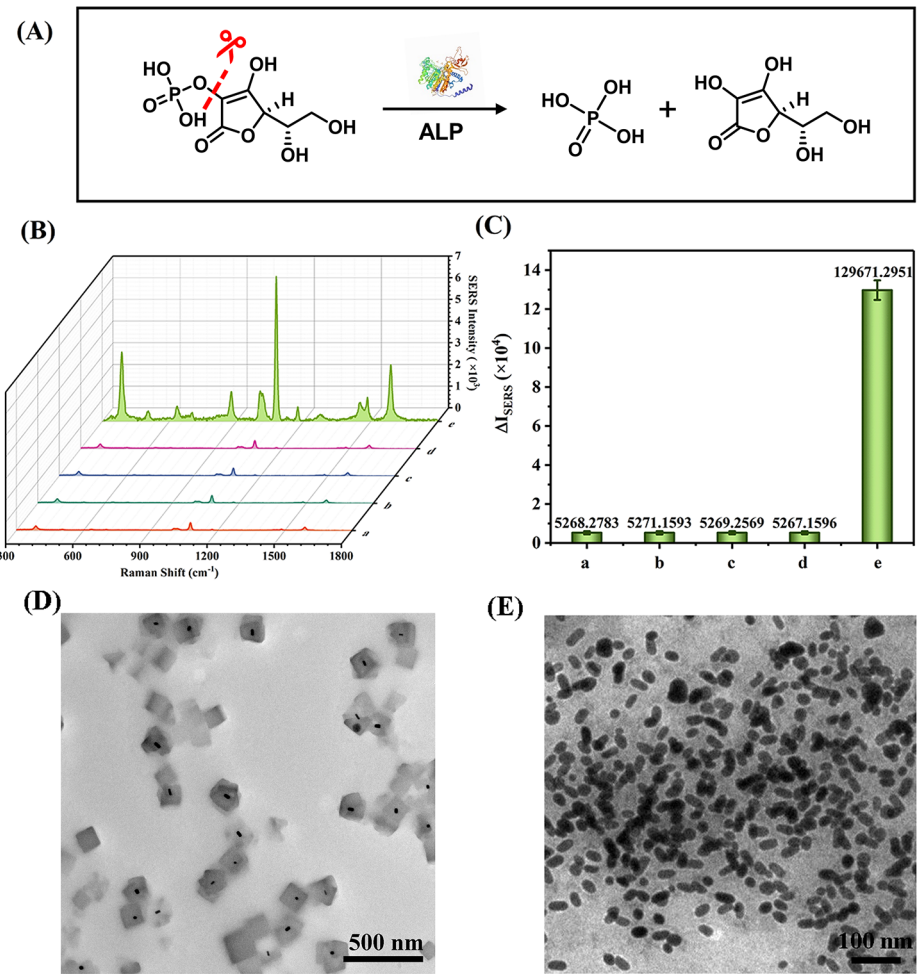

Figure 3. Reaction between AA2P and ALP (A). SERS spectra of PAZ NPs incubated with AA (a), AA2P (b), ALP (c), AA and ALP (d), and AA2P and ALP (e) (B). Difference of the SERS peak area of PAZ NPs incubated with AA (a), AA2P (b), ALP (c), AA and ALP (d), and AA2P and ALP (e) (C). TEM images of PAZ NPs before (D) and after (E) enzymatic hydrolysis.

decomposition of ZIF-8. In addition, under alkaline conditions, AA cannot be easily destroyed, whereas ALP is more active. Therefore, HEPES at pH = 8.5 not only can eliminate the influence of AA on the experiment but also can minimize the influence of ionic strength on the nanoparticle solution.

Figure 2A shows that the cubic ZIF-8 nanocrystals were successfully synthesized, and Figure 2B–D shows that ZIF-8 was etched with Pi, as its relatively smooth surface became rough. With the increase in phosphate concentration, the etching degree of ZIF-8 gradually increased. When the phosphate concentration reached 5 mM, ZIF-8 was completely decomposed (Figure 2D). To demonstrate that phosphate can decompose ZIF-8, we introduced sodium phosphate into the strategy to directly demonstrate that Pi can lead to the degradation of PAZ NPs (Figure S9).

From a mechanistic point of view, the degradation of ZIF-8 can occur in water only during the first few hours while can gradually reach equilibrium thereafter, and the degree of degradation depends on the initial concentration of ZIF-8.[33] Compared with that in water, the degradation rate of ZIF-8 in PBS solution is faster, and the degradation degree is also higher. This is due to the strong affinity between Pi and Zn^{2+}, resulting in the breakage of the link between Zn^{2+} and MIM^{-}.

In water, the hydration–deprotonation equilibrium can be represented by the following reaction:

$$Zn(MIM)_2 + 2H_2O \leftrightarrow Zn^{2+} + 2H\,MIM + 2OH^{-} \quad (1)$$

The affinity of phosphate ions in PBS toward the degradation product of ZIF-8 can be expressed as follows:

$$3Zn^{2+} + 2PO_4^{3-} + 4H_2O \leftrightarrow Zn_3(PO_4)_2(H_2O)_4 \quad (2)$$

Since free Zn^{2+} can form new zinc compounds with PO_4^{3-} (eq 2), its concentration then decreases, causing the degradation balance to shift to the right (eq 1); as a result, the degradation of ZIF-8 is promoted.

Furthermore, as can be seen in Figure 2E,F after Pi was added, the structure of ZIF-8 was severely damaged, and PATP-Au NPs were released causing them to become aggregated, which in turn increased SERS "hot spot" areas and SERS signals. The synchronous fluorescence spectra and SERS spectra were measured in PBS solution at different concentrations, as shown in Figure 2G. It was found that the peak height of the synchronous fluorescence spectra decreased with the increase of the PBS solution concentration, indicating that the scattering in the mixed solution was weakened, proving that the structure of ZIF-8 could be broken by Pi. According to the XRD pattern (Figure 1D), when PBS solution was introduced into ZIF-8 solution and PAZ NP solution, the characteristic peaks of ZIF-8 disappeared, which

https://doi.org/10.1021/acs.analchem.2c05098
Anal. Chem. 2023, 95, 3414–3422

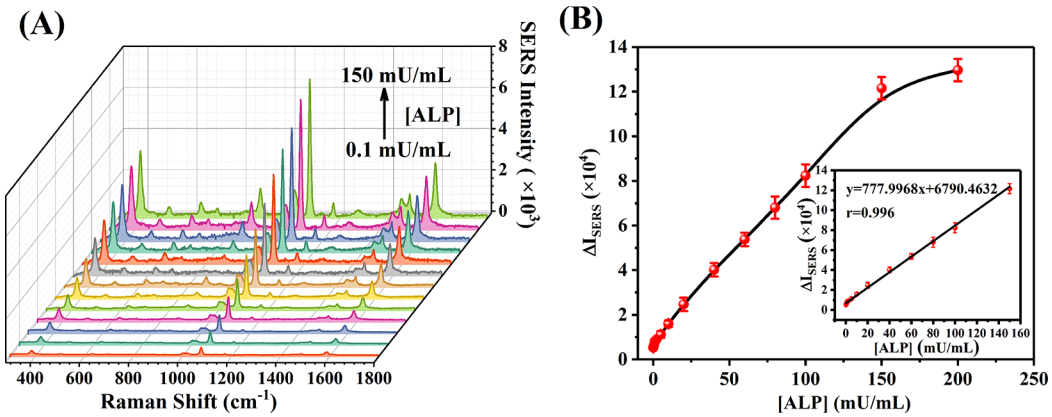

Figure 4. SERS response of PAZ NPs in the presence of ALP at various concentrations (A). Linear relationship between the SERS intensity and ALP concentration (n = 3) (B).

Table 1. Comparison of the Developed Method with Other Reported Methods

materials	instruments	time (s)	determination of ALP: linear range (mU/mL)	determination of ALP: detection limit (mU/mL)	ref.
Au@BCIP NPs[a]	LabRAM ARAMIS Raman spectrometer (Horiba Jobin Yvon)	10	1.0−50.0	1.0	41
4-MPBA-Au@Ag NPs[b]	DXR Raman microscope spectrometer (Thermo Fisher)		0.5−10.0	0.1	42
AMAM[c]	InVia Raman microscope spectrometer (Renishaw)	10	0.1−70.0	0.079	43
AMNS[d]	LabRAM HR Evolution microscope spectrometer (Horiba Jobin Yvon)	10	0.4−20.0	0.04	44
ABA NPs[e]	InVia Plus Raman microscope spectrometer (Renishaw)		0.72−3.00	0.01	22
PAZ NPs[f]	i-Raman plus portable spectrometer (B&W TEK)	3	0.1−150.0	0.03	this work

[a]Au@BCIP NPs: 5-bromo-4-chloro-3-indolyl phosphate-modified gold nanoparticles. [b]4-MPBA-Au@Ag NPs: 4-mercaptophenylboronic acid-modified silver-coated gold nanoparticles. [c]AMAM: MnO_2 shell-isolated 4-mercaptopyridine-modified gold nanoparticles. [d]AMNS: gold nanobipyramids@MnO_2 nanoparticles. [e]ABA NPs: alkyne-coded bis(p-sulfonatophenyl) phenylphosphine dihydrate dipotassium salt-protected gold nanoparticles. [f]PAZ NPs: PATP-Au@ZIF-8 nanoparticles.

is the indication that Pi can cause the ZIF-8 structure to collapse.

It can be seen from the SERS spectra (Figure 2H) that as the concentration of PBS solution increased, the characteristic peaks at 1075 cm^{-1} gradually increased, which further verifies that Pi can cause the structure of ZIF-8 to collapse, and the release of PATP-Au NPs can provide a stronger SERS activity, resulting in the enhancement of SERS intensity. As designed, with the increase of the ALP activity, the degree of hydrolysis of AA2P increases, and more Pi is generated, which further enhances the intensity of the SERS signal at 1075 cm^{-1}.

Control of ZIF-8 Collapse and PATP-Au NP Release by ALP. Pi can be generated by hydrolysis of AA2P self-triggered as a result of the presence of ALP (Figure 3A). Because AA2P could be hydrolyzed to AA and Pi in the presence of ALP, we considered the influence of AA, AA2P, and ALP on the experiment. We added AA (10 mM), AA2P (10 mM), or ALP (200 mU/mL) into the solution of PAZ NPs, before adding HEPES buffer to adjust its pH to 8.5. AA has strong reducibility; thus, too much of its content can cause the solution to have an acidic pH. An acidic pH can cause the collapse of the ZIF-8 structure.[38,39]

In addition, the effect of the AA2P substrate and ALP on the SERS intensity was investigated. As shown in Figure 3B, the SERS intensity of PAZ NPs incubated with AA and AA2P was not significantly changed, indicating that AA and the phosphate group in AA2P cannot decompose ZIF-8 and trigger the release of PATP-Au NPs. Similarly, PAZ NPs did not respond to the presence of ALP alone (Figure 3B). In the presence of ALP and AA2P, the SERS intensity increased, indicating that the release of PATP-Au NPs was initiated (Figure 3C). ΔI_{SERS} represents the difference of SERS intensities at 1075 cm^{-1}. These results prove that individual AA2P, AA, or ALP had no effect on the experiment, and the increase of SERS intensity was due to phosphate produced as a result of AA2P hydrolysis by ALP, which is the mechanism that lays the foundation for ALP determination. As can be seen in Figure 3D,E, after ALP was added, PATP-Au NPs were released causing them to become aggregated, which in turn causes the SERS "hot spot" areas and SERS signals to increase. It can be inferred that our SERS method has superior performance in assaying ALP.

Performance of Self-Triggered Control of Collapse of the Metal Framework Structure. Based on the above experimental verification, we established a strategy to realize the ALP-induced self-triggering control by establishing a physical shell (ZIF-8) on the surface of Au NPs. Pi can be generated by hydrolysis of AA2P self-triggered as a result of the presence of ALP and decompose ZIF-8 through coordination with Zn^{2+} and thus can destroy the ZIF-8 shell structure of the prepared PAZ NPs. Au NPs are released and then become aggregated, leading to the increase of the SERS "hot spot" area and SERS signals.

Under the optimal experimental conditions, calibration curves for the method were constructed by using the developed SERS strategy. Corresponding descriptions and

https://doi.org/10.1021/acs.analchem.2c05098
Anal. Chem. 2023, 95, 3414−3422

Table 2. Result of ALP Detection in Human Serum Samples (n = 3)

samples	ALP kit (mU/mL)	this work (mU/mL)	relative error (%)	added (mU/mL)	found (mU/mL)	recovery (%)
1	53.36 ± 2.32	55.13 ± 0.85	103.32	20	71.98 ± 1.41	98.12
2	59.61 ± 1.74	57.98 ± 2.59	97.27	20	77.51 ± 2.16	97.36
3	65.28 ± 0.97	66.52 ± 1.24	101.90	20	88.33 ± 1.96	103.58

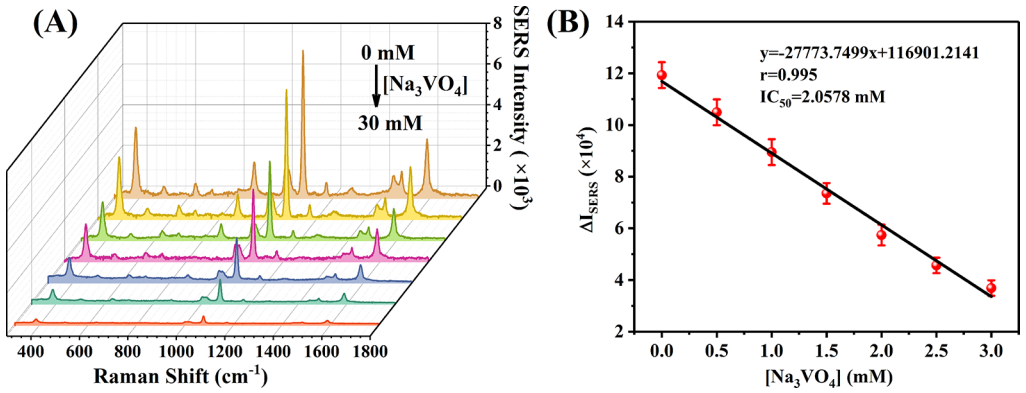

Figure 5. SERS spectra of Na_3VO_4-treated ALP (A). Linear relationship between the SERS intensity and Na_3VO_4 concentration (n = 3) (B).

figures are given in the Supporting Information (Figure S4). As the ALP concentration increased from 0 to 200 mU/mL, the SERS intensity at 1075 cm^{-1} gradually increased. The correlation had excellent linearity at ALP concentrations ranging from 0.1 to 150 mU/mL with a regression equation $y = 777.9968x + 6790.4632$ (correlation coefficient $r = 0.996$) (Figure 4B). The limit of detection (LOD) was 0.03 mU/mL (error bars indicate standard deviations (n = 3)).

These results indicate that the SERS method could effectively determine the ALP activity. Compared with other methods (Table 1), our strategy has a wider linear range and a higher sensitivity, and the detection limit of our strategy is comparable or lower than other methods. In addition, as can be seen in Table 1, the detections of ALP by SERS methods were accomplished by large-scale Raman systems. The prices of such systems are high, which may limit the application of SERS technology in the screening of related diseases. By contrast, a portable Raman spectrometer has the advantages of small size, low price, and on-site detection capacity. Compared with other large-scale Raman system-based ALP detection methods, our method utilized a portable Raman spectrometer, which has lower or equivalent detection sensitivity and shorter detection time, thus meeting the requirements of accurate and rapid clinical testing.[40]

The reproducibility and stability of SERS substrates are important indicators for the construction of sensors. To investigate the preparation reproducibility of the PAZ NP substrate preparation, Figure S7 shows a histogram of the difference of SERS intensity at 1075 cm^{-1} displacement for 5 different batches of PAZ NPs incubated with PBS (10 mM). It can be seen from the figure that the relative standard deviation (RSD) value of the signal intensity at the displacement of 1075 cm^{-1} is 2.31%, indicating that the MOF-based SERS substrates have good preparation reproducibility. To evaluate the SERS stability of PAZ NPs, the difference of SERS intensity at 1075 cm^{-1} on the PAZ NP substrate under different storage times (1−15 days) was observed (Figure S8). The SERS intensity of the PAZ NPs showed only a slight attenuation (9.4%) after 15 days of storage and still had an acceptable RSD value (6.7%) from multiple measurements (n = 5). The above results demonstrated the reproducibility and storage stability of the SERS platform using PAZ NPs as a substrate, as well as its potential of quantitative detection, which were of great significance for practical analysis.

Applications of PAZ NPs as an Alkaline Phosphatase Sensor for Human Serum. The selectivity is a key parameter reflecting the applicability of a sensing strategy in detecting complex real samples. In this experiment, the specific response of PAZ NPs to ALP in the presence of several enzymes (trypsin (TPS), lysozyme (LZM), acid phosphatase (ACP), and acetylcholinesterase (AChE)) and biomolecules (glucose (Glu), tyrosine (Tyr), bovine serum albumin (BSA), and adenosine triphosphate (ATP)) was investigated. As shown in Figure S5A, the SERS signal was changed or highly enhanced only in the presence of ALP, which indicates that the designed PAZ NP sensing strategy is selective to the target ALP.

In addition, we assessed the anti-interference ability of PAZ NPs. In the anti-interference experiment, the specific response of PAZ NPs to Pi in the presence of several inorganic ions, enzymes, and biomolecules was investigated. As shown in Figure S5B, incubation with interferences and ALP did not lead to a remarkable signal change, which is indicative that the designed PAZ NP sensing system has a good anti-interference ability and is only specific to the target ALP. It has been reported that ATP can disintegrate ZIF-8 in Tris (5 mM) buffer, pH = 7.4.[45] However, in this work, no prominent change was observed when ATP was used, possibly due to the difference between the reaction conditions, e.g., the optimal reaction pH used in our work was pH = 8.5, and HEPES was used as a buffer.

With its linear range within the levels of the ALP activity commonly found in human serum (40−190 mU/mL),[46] our SERS strategy was employed to directly test a mixed solution containing undiluted serum and the probe. Table 2 shows that the detection results obtained from the SERS method were comparable to those obtained from commercial ALP kits. The relative errors between SERS and ELISA quantification were less than 103.32%, indicating that the SERS sensing strategy could accurately detect ALP. In addition, the averaged recoveries of spiked ALP were in the range of 97.36 to

https://doi.org/10.1021/acs.analchem.2c05098
Anal. Chem. 2023, 95, 3414−3422

103.58%, indicating that our sensing strategy can reliably be employed in quantitative analysis of undiluted serum samples. In order to verify that the strategy has the detection ability in samples with lower concentrations of ALP, we investigated the spike experiments of diluted samples (Table S1). The averaged recoveries of spiked ALP in diluted serum were in the range of 97.38 to 104.81%, indicating that our sensing strategy also has a certain application potential at lower concentrations of ALP.

Applications of PAZ NPs as an Alkaline Phosphatase Inhibitor Sensor. To confirm its effectiveness in screening inhibitors, the proposed strategy was employed to screen the ALP inhibitor (Na_3VO_4).[47] The half-maximal inhibitory concentration, or the half-inhibition rate, or IC_{50}, is crucial data used to evaluate the effectiveness of inhibitors. At a constant ALP activity (200 mU/mL), the SERS intensity decreased with an increasing Na_3VO_4 concentration, clearly demonstrating that Na_3VO_4 has an inhibitory effect on ALP in a concentration-dependent manner (Figure 5). As depicted in Figure 5B, the relationship between the ΔI_{SERS} value and the Na_3VO_4 concentration was linear. As detected by the developed SERS strategy, the IC_{50} value required for Na_3VO_4 to inhibit 200 mU/mL ALP was 2.0578 mM, which is consistent with the value reported in the literature.[48] These results essentially indicate that the strategy, in which PAZ NPs were used as nanoprobes, developed in this study could be used to evaluate the effect of inhibitors on an enzyme.

CONCLUSIONS

In summary, core−shell metal−organic framework composites were developed as SERS substrates and used for the determination of the ALP activity and ALP inhibitors. This strategy can effectively avoid the potentially inaccurate ALP measurement results obtained by some commonly used methods that detect AA generated by ALP. Because free phosphate ions (Pi), of which the generation is self-triggered by the presence of ALP, can cause the disintegration of ZIF-8 by coordinating with Zn^{2+}, they can destroy the core−shell structure of the prepared PAZ NPs. This in turn leads to exposure of internal Au NPs and the increase of the SERS "hot spot" area, which allow for the sensitive SERS detection of ALP in real samples. The response of the SERS strategy was linear at ALP concentrations ranging from 0.1 to 150 mU/mL (r = 0.996), and its detection limit was 0.03 mU/mL. The strategy developed in this study was further employed in the screening of ALP inhibitors. All SERS measurements were performed using portable Raman spectrometers. The possibility to implement the developed SERS substrate in the rapid and selective analysis of ALP in human serum was also demonstrated.

ASSOCIATED CONTENT

Supporting Information

The Supporting Information is available free of charge at https://pubs.acs.org/doi/10.1021/acs.analchem.2c05098.

Additional experimental details, including instruments and reagents, synthesis, phosphate-controlled collapse of ZIF-8, selectivity evaluation, quantitative detection of the ALP activity, determination of ALP in serum, evaluation of the ALP inhibitor, SERS measurement, scheme of synthesis of PAZ NPs, characterization of PAZ NPs synthesized without CTAB, SERS spectra of PATP-Au NPs and PAZ NPs, condition optimization for PAZ NP construction, selectivity and anti-interference experiments, photos of PAZ NPs, Au NPs, and ZIF-8 solutions, preparation reproducibility experiments, storage stability experiment, result of ALP detection in diluted serum samples (PDF)

AUTHOR INFORMATION

Corresponding Authors

Pinyi Ma − *College of Chemistry, Jilin Province Research Center for Engineering and Technology of Spectral Analytical Instruments, Jilin University, Changchun, Jilin 130012, China*; orcid.org/0000-0002-3230-4928; Email: mapinyi@jlu.edu.cn

Daqian Song − *College of Chemistry, Jilin Province Research Center for Engineering and Technology of Spectral Analytical Instruments, Jilin University, Changchun, Jilin 130012, China*; orcid.org/0000-0002-4866-1292; Email: songdq@jlu.edu.cn

Authors

Wei Wang − *College of Chemistry, Jilin Province Research Center for Engineering and Technology of Spectral Analytical Instruments, Jilin University, Changchun, Jilin 130012, China*

Jingkang Li − *College of Chemistry, Jilin Province Research Center for Engineering and Technology of Spectral Analytical Instruments, Jilin University, Changchun, Jilin 130012, China*

Yibing Liu − *College of Chemistry, Jilin Province Research Center for Engineering and Technology of Spectral Analytical Instruments, Jilin University, Changchun, Jilin 130012, China*

Wei Zhang − *College of Chemistry, Jilin Province Research Center for Engineering and Technology of Spectral Analytical Instruments, Jilin University, Changchun, Jilin 130012, China*

Ying Sun − *College of Chemistry, Jilin Province Research Center for Engineering and Technology of Spectral Analytical Instruments, Jilin University, Changchun, Jilin 130012, China*

Complete contact information is available at: https://pubs.acs.org/10.1021/acs.analchem.2c05098

Notes

The authors declare no competing financial interest.

ACKNOWLEDGMENTS

This work was supported by the National Natural Science Foundation of China (22004046 and 22074052).

REFERENCES

(1) Lorenz, B.; Schröder, H. C. *Biochim. Biophys. Acta, Protein Struct. Mol. Enzymol.* **2001**, *1547*, 254−261.

(2) Tsai, L. C.; Hung, M. W.; Chen, Y. H.; Su, W. C.; Chang, G. G.; Chang, T. C. *Eur. J. Biochem.* **2000**, *267*, 1330−1339.

(3) Trowsdale, J.; Martin, D.; Bicknell, D.; Campbell, I. *Biochem. Soc. Trans.* **1990**, *18*, 178−180.

(4) Wang, K.; Jiang, L.; Zhang, F.; Wei, Y.; Wang, K.; Wang, H.; Qi, Z.; Liu, S. *Anal. Chem.* **2018**, *90*, 14056−14062.

(5) Huang, S.; Yang, W.; Ye, S.; Cao, S.; Li, Y.; Wei, Z.; Yan Ngai, K.; Dai, J.; Mao, G.; Ma, Y. *Spectrochim. Acta, Part A* **2022**, *280*, 121550.

(6) Heazell, A. E. P.; Judge, J. K.; Bhatti, N. R. *J. Matern.-Fetal Neonat. Med.* **2006**, *19*, 311−313.
(7) Liang, Y.; Zeng, T.; Tian, J.; Yan, J.; Lan, Z.; Chen, J.; Xin, X.; Lei, B.; Cai, Z. *Sci. Total Environ.* **2021**, *798*, 149379.
(8) Yuan, T.; Shi, C.; Xu, W.; Yang, H.-L.; Xia, B.; Tian, C. *Endocr. J.* **2021**, *68*, 1197−1208.
(9) Mahato, K.; Chandra, P. *Biosens. Bioelectron.* **2019**, *128*, 9−16.
(10) Asadi, M.; Babamiri, B.; Hallaj, R.; Salimi, A. *J. Electroanal. Chem.* **2022**, *914*, 116306.
(11) Wang, X.-Y.; Wu, M.-X.; Ding, S.-N. *Chem. Commun.* **2020**, *56*, 8099−8102.
(12) Wang, W.; Zhang, Y.; Zhang, W.; Liu, Y.; Ma, P.; Wang, X.; Sun, Y.; Song, D. *Anal. Chim. Acta* **2021**, *1183*, 338989.
(13) Zhao, X.; Zhao, S.; Song, Z.-L.; Zhang, X.; Zhang, S.; Song, W.; Chen, Z. *Sens. Actuators, B* **2021**, *331*, 129373.
(14) Cao, F.; Wang, M.; Yi, X.; Sun, D. *Analyst* **2022**, *147*, 2494−2499.
(15) Zong, C.; Chen, C.-j.; Wang, X.; Hu, P.; Liu, G.-k.; Ren, B. *Anal. Chem.* **2020**, *92*, 15806−15810.
(16) Piao, L.; Park, S.; Lee, H. B.; Kim, K.; Kim, J.; Chung, T. D. *Anal. Chem.* **2010**, *82*, 447−451.
(17) Wang, C.; Gao, Y.; Hu, S.; Zhu, A.; Ying, Y.; Guo, X.; Wu, Y.; Wen, Y.; Yang, H. *Biosens. Bioelectron.* **2022**, *215*, 114388.
(18) Ma, H.; Han, X. X.; Zhao, B. *TrAC, Trends Anal. Chem.* **2020**, *131*, 116019.
(19) Zhu, T.; Chen, J.; Chai, Q.; Zeng, S.; Liu, Y. *Anal. Chim. Acta* **2022**, *1232*, 340453.
(20) Zhao, Y.; Wang, R.; Xue, Y.; Jie, G. *Sens. Actuators, B* **2022**, *369*, 132397.
(21) Xi, C.-Y.; Zhang, M.; Jiang, L.; Chen, H.-Y.; Lv, J.; He, Y.; Hafez, M. E.; Qian, R.-C.; Li, D. W. *Sens. Actuators, B* **2022**, *369*, 132264.
(22) Liu, H.; Wei, L.; Hua, J.; Chen, D.; Meng, H.; Li, Z.; Xiao, L. *Nanoscale* **2020**, *12*, 10390−10398.
(23) Hornig, D. *Ann. N. Y. Acad. Sci.* **1975**, *258*, 103−118.
(24) Sakagami, H.; Satoh, K.; Ohata, H.; Takahashi, H.; Yoshida, H.; Iida, M.; Kuribayashi, N.; Sakagami, T.; Momose, K.; Takeda, M. *Anticancer Res.* **1996**, *16*, 2635−2644.
(25) Zhang, W.; Cui, X.; Wang, D.; Liu, Y.; Yong, L.; Li, N.; Jia, X. *J. Nutr., Health Aging* **2012**, *16*, 442−444.
(26) Fu, Q.; Li, Z.; Fu, F.; Chen, X.; Song, J.; Yang, H. *Nano Today* **2021**, *36*, 101014.
(27) Li, W.; Kanyo, I.; Kuo, C.-H.; Thanneeru, S.; He, J. *Nanoscale* **2015**, *7*, 956−964.
(28) Masoomi, M. Y.; Morsali, A.; Dhakshinamoorthy, A.; Garcia, H. *Angew. Chem., Int. Ed.* **2019**, *58*, 15188−15205.
(29) Chen, L.; Liu, D.; Peng, J.; Du, Q.; He, H. *Coord. Chem. Rev.* **2020**, *404*, 213113.
(30) Mehek, R.; Iqbal, N.; Noor, T.; Amjad, M. Z. B.; Ali, G.; Vignarooban, K.; Khan, M. A. *RSC Adv.* **2021**, *11*, 29247−29266.
(31) Zheng, C.; Qiu, X.; Han, J.; Wu, Y.; Liu, S. *ACS Appl. Mater. Interfaces* **2019**, *11*, 42243−42249.
(32) He, Z.; Huang, X.; Wang, C.; Li, X.; Liu, Y.; Zhou, Z.; Wang, S.; Zhang, F.; Wang, Z.; Jacobson, O.; Zhu, J.-J.; Yu, G.; Dai, Y.; Chen, X. *Angew. Chem., Int. Ed.* **2019**, *58*, 8752−8756.
(33) Taheri, M.; Ashok, D.; Sen, T.; Enge, T. G.; Verma, N. K.; Tricoli, A.; Lowe, A. R. D.; Tsuzuki, T. *Chem. Eng. J.* **2021**, *413*, 127511.
(34) Hu, P.; Zhuang, J.; Chou, L.-Y.; Lee, H. K.; Ling, X. Y.; Chuang, Y.-C.; Tsung, C.-K. *J. Am. Chem. Soc.* **2014**, *136*, 10561−10564.
(35) Izadpanah Ostad, M.; Niknam Shahrak, M.; Galli, F. *J. Co2 Utili* **2021**, *43*, 101373.
(36) Gou, L.; Zeng, X.; Du, H.; Li, L.; Tian, Y.; Hou, X.; Wu, L. *Talanta* **2022**, *237*, 122925.
(37) Shi, C.; Qin, L.; Wu, S.; Kang, S.-Z.; Li, X. *Chem. Eng. J.* **2021**, *422*, 129970.
(38) Yao, T.; Feng, J.; Chu, C.; Ma, Z.; Han, H. *Sens. Actuators, B* **2021**, *348*, 130701.
(39) Abd Al-jabbar, S.; Atiroğlu, V.; Hameed, R. M.; Guney Eskiler, G.; Atiroğlu, A.; Deveci Ozkan, A.; Özacar, M. *Bioorg. Chem.* **2022**, *118*, 105467.
(40) Wang, W.; Ma, P.; Song, D. *Luminescence* **2022**, *37*, 1822−1835.
(41) Sun, D.; Xu, W.; Liang, C.; Shi, W.; Xu, S. *ACS Sens.* **2020**, *5*, 1758−1767.
(42) Zhang, J.; He, L.; Zhang, X.; Wang, J.; Yang, L.; Liu, B.; Jiang, C.; Zhang, Z. *Sens. Actuators, B* **2017**, *253*, 839−845.
(43) Dai, X.; Lu, L.; Zhang, X.; Song, Z.-L.; Song, W.; Chao, Q.; Li, Q.; Wang, W.; Chen, J.; Fan, G.-C.; Luo, X. *Sens. Actuators, B* **2021**, *334*, 129605.
(44) Zeng, Y.; Ren, J.-Q.; Wang, S.-K.; Mai, J.-M.; Qu, B.; Zhang, Y.; Shen, A.-G.; Hu, J.-M. *ACS Appl. Mater. Interfaces* **2017**, *9*, 29547−29553.
(45) Zhou, X.; Li, J.; Tan, L.-L.; Li, Q.; Shang, L. *J. Mater. Chem. B* **2020**, *8*, 3661−3666.
(46) Deligianni, D. D.; Katsala, N. D.; Koutsoukos, P. G.; Missirlis, Y. F. *Biomaterials* **2001**, *22*, 87−96.
(47) Zhan, Y.; Yang, S.; Chen, L.; Zeng, Y.; Li, L.; Lin, Z.; Guo, L.; Xu, W. *ACS Sustainable Chem. Eng.* **2021**, *9*, 12922−12929.
(48) Deng, J.; Yu, P.; Wang, Y.; Mao, L. *Anal. Chem.* **2015**, *87*, 3080−3086.

https://doi.org/10.1021/acs.analchem.2c05098
Anal. Chem. 2023, 95, 3414−3422